THE JOURNAL OF PHYSICAL CHEMISTRY B
A JOURNAL OF THE AMERICAN CHEMICAL SOCIETY

pubs.acs.org/JPCB

Article

# Nanopumps without Pressure Gradients: Ultrafast Transport of Water in Patterned Nanotubes

Ermioni Papadopoulou, Constantine M. Megaridis, Jens H. Walther, and Petros Koumoutsakos*

Cite This: https://doi.org/10.1021/acs.jpcb.1c07562

Read Online

ACCESS | Metrics & More | Article Recommendations | Supporting Information

**ABSTRACT:** The extreme liquid transport properties of carbon nanotubes present new opportunities for surpassing conventional technologies in water filtration and purification. We demonstrate that carbon nanotubes with wettability surface patterns act as nanopumps for the ultrafast transport of picoliter water droplets without requiring externally imposed pressure gradients. Large-scale molecular dynamics simulations evidence unprecedented speeds and accelerations on the order of $10^{10}$ g of droplet propulsion caused by interfacial energy gradients. This phenomenon is persistent for nanotubes of varying sizes, stepwise pattern configurations, and initial conditions. We present a scaling law for water transport as a function of wettability gradients through simple models for the droplet dynamic contact angle and friction coefficient. Our results show that patterned nanotubes are energy-efficient nanopumps offering a realistic path toward ultrafast water nanofiltration and precision drug delivery.

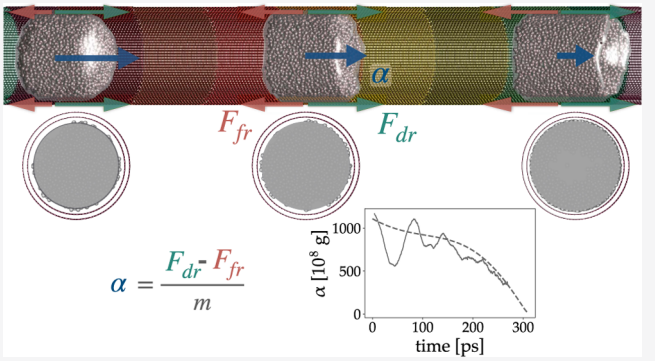


## INTRODUCTION

Fast transport of liquids through nanometer-sized conduits is fundamental for the advancement of nanomedicine,[1] nanosensing,[2] and nanofiltration.[3−5] Nanoporous membranes fabricated from arrays of carbon nanotubes (CNTs) or boron nitride nanotubes (BNNTs) are considered compatible materials for usage as components of nanofilters and biosensors.[6] Carbon nanotubes in aqueous environments[7,8] exhibit excellent osmotic[9−11] and permselectivity[12,13] properties, with their water permeability found to be highly dependent on the nanopore radius.[14,15]

The key characteristic of these nanofluidic systems is the large ratio of the interfacial area with respect to the liquid volume. This ratio highlights the importance of local interfacial phenomena to fluid transport characteristics.[16] The response of water in the proximity of graphitic interfaces at the nanoscale has been found to deviate from bulk behavior for static and dynamic properties of confined water[7,17] due to local variations of the structural order of water owing to the interaction with the solid surface.[18,19] The exploration of osmotic capabilities of graphitic nanomembranes has revealed a curvature-dependent slippage mechanism,[20−22] attributed to the inherent ultralow friction of water in CNTs.[23,24] Several theoretical and modeling approaches have focused on quantifying the slip length in CNTs.[14,20] However, the quantification of the water friction and transport mechanism in nanomembranes remains incomplete, as no model accounts for the effects of both curvature and surface properties.

The structural and dynamical behavior of interfacial water is known to depend on the chemical composition of the confining material, which designates the surface wettability,[25] i.e., the affinity between the surface and the fluid. In recent years, the ability to tune surface properties[26,27] and pattern nanoscale interfaces[28] has become a critical component for several emerging applications for liquid and gas transport.[29] Nanoscale surface energy gradients can greatly affect the nanoscale liquid transport through thermophoretic[30−33] and electroosmotic[12,34−36] effects, while structural modifications of nanotube ends have shown to enhance their permselectivity.[37]

Surface chemical engineering has the potential to tinker nanoscale flow characteristics.[38−40] Flows in nanochannels and nanotubes depend on the wall wettability,[41−47] and wettability gradients have been shown to maintain continuous flow in channels of patterned graphene.[48] Tuning surface properties[26,27] allows for drastic flow modifications at the nanoscale.[29] Inspired by natural patterns, previous experiments[49,50] and simulations[51] have demonstrated ultrafast transport of droplets on patterned graphene. Moreover, recent simulations have

Received: August 26, 2021
Revised: October 5, 2021

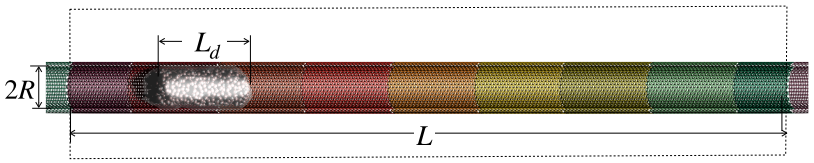


| Zone | 1 | 2 | 3 | 4 | 5 | 6 | 7 | 8 | 9 |
|---|---|---|---|---|---|---|---|---|---|
| $\epsilon_{CO}$ [kcal/mol] | 0.040 | 0.055 | 0.070 | 0.085 | 0.100 | 0.115 | 0.130 | 0.145 | 0.160 |
| $\theta_S$ [°] | 147 | 132 | 117 | 102 | 88 | 73 | 58 | 44 | 29 |

**Figure 1.** Baseline nanotube system used in this study. The CNT has length $L$ = 50 nm and inner radius $R$ = 1.356 nm. The water droplet length is $L_d$ = 6 nm. The boundaries of the periodic domain are marked with a dotted black line. The periodic images of the system in the axial direction of the nanotube are shown with faded colors outside the periodic domain boundaries. The wettability of each annular zone is described in the table below the image, where zone 1 corresponds to the purple-colored zone on the left-hand side in this figure, and zone 9 corresponds to the dark-green-colored zone on the right-hand side. The wettability of each spatial zone is defined with a different interaction strength $\epsilon_{CO}$ between carbon and water corresponding to the respective equilibrium contact angle $\theta_S$ of the droplet.

evidenced active control of water transport through nanopores by temporal modifications of the surface hydrophobicity.[52]

Here, we demonstrate for the first time that spatially varying hydrophobicity patterns in the interior of carbon nanotubes produce ultraefficient nanopumps. We develop a model of droplet transport and show that the friction forces on the moving droplet scale with its size. We introduce scaling laws for the friction and the dynamic contact angle of the confined droplet in terms of the CNT curvature and the surface wettability. These scaling laws rationalize the dynamics of a moving droplet under the influence of surface wettability gradients along nanotubes.

## METHODS

We perform MD simulations of systems of water droplets confined into periodic rigid double-walled carbon nanotubes (DW-CNTs) with a surface energy gradient along their main axis and study the transport characteristics of these droplets. Scaling of the forcing and transport characteristics is attempted, and results for nanotubes of different lengths and radii are compared to a baseline case, which consists of a (20, 20)@(25, 25) CNT with inner radius 1.365 nm and length $L$ = 50 nm (see Figure 1).

The surface energy pattern along the CNT main axis is defined through nine zones, each of different wettability. We tune the wettability of each spatial zone through the solid−liquid interaction strength $\epsilon_{CO}$ that describes the nonbonded interaction of the carbon and the oxygen atoms.[53,54] Throughout this study, we have chosen to work with a discretized stepwise gradient of surface wettability along the CNT length, which is easier to model and has proven to produce extremely efficient droplet transport on similarly patterned flat graphene.[51] The pattern is constructed with an increasing wettability along the length of the CNT, starting from a hydrophobic band with a corresponding contact angle of 147° and leading to a hydrophilic band with a contact angle of 29°, with a higher interaction energy between carbon and oxygen atoms, $\epsilon_{CO}$ (see Figure 1).

The water droplets for all simulation cases are equilibrated in the isothermal−isochoric (NVT) ensemble in a CNT of neutral wettability, with interaction strength $\epsilon_{CO}$ = 0.09369 kcal/mol, corresponding to an equilibrium contact angle of ≈90° (cf. ref 51) with a flat graphene sheet and of the same length as the respective simulation case (see SI, Section 1.1).

In the baseline case, the droplet consists of 838 water molecules and its length is $L_d$ = 6 nm, defining an aspect ratio of the droplet length to the tube length of 0.12. The entire set of systems in this study maintains the same aspect ratio, which translates to a constant wettability gradient throughout the study, making it easier to quantify the effects of friction and Laplace forces with respect to droplet size.

The interactions of water molecules are modeled with the TIP4P-Ew model.[55] The particle−particle particle-mesh (P3M) algorithm is used to compute the long-range electrostatic interactions, with a root-mean-squared accuracy of $10^{-5}$ (cf. ref 56 in the force calculation). The SHAKE algorithm is used to constrain the molecular structure of the water molecules.[57] For short-range interactions, we use a cutoff of 1.0 nm for the C−O pair (cf. ref 58) and a cutoff of 0.9 nm for the O−O pair (cf. ref 59). A sensitivity analysis shows that a 20% reduction of the cutoff distance results in a 10% reduction of the maximum center-of-mass (CoM) velocity of the droplet (see SI, Section 1.2). For the P3M algorithm used for the long-range electrostatic interactions, we set the cutoff distance at 0.85 nm.[55]

The nonbonded interaction between the carbon atoms and the water molecules is modeled with a 12-6 Lennard-Jones potential $U_{CO}(r) = 4\epsilon_{CO}[(\sigma_{CO}/r)^{12} - (\sigma_{CO}/r)^{6}]$, where $\epsilon_{CO}$ is the interaction strength responsible for varying the surface wettability and $r$ is the distance between two atoms. The parameter $\sigma_{CO}$ is considered constant and equal to 3.296 Å.

The carbon atoms are considered rigid for all simulations, if not stated otherwise, to eliminate any other effects, except for the wettability gradient effect.[60,61] Kou et al.[47] studied the effect of wettability gradients for flexible single-walled CNTs. They recovered a 40% reduction of the maximum $V_{CoM}$ for a CNT with a surface energy pattern in the hydrophilic regime. We test how the phonon excitation of the carbon nanotubes affects the results in the present study and find that the maximum CoM velocity of a water droplet in a flexible CNT with the same wettability gradient varies up to 10%, while the corresponding acceleration of the droplet varies up to 10% (see SI, Section 1.4).

All MD simulations are carried out using the molecular dynamics package LAMMPS[62] with a time step of 1 fs. All visualizations are performed with the use of the visual molecular dynamics (VMD) package.[63] The preparation of the patterned carbon nanotubes is performed with the package


https://doi.org/10.1021/acs.jpcb.1c07562
J. Phys. Chem. B XXXX, XXX, XXX−XXX

WCCNT developed within the CSE-Lab.[64] Postprocessing of the results has been partially performed using the package MDAnalysis.[65] Preparation of the systems, including defining the various wettability zones on the CNTs, is also performed with TCL-scripting within the VMD package.

Furthermore, to better assess the kinetics of the droplet motion, constrained MD simulations are conducted, aiming to measure the friction force acting on a water droplet due to wettability variations in CNTs. For the computation of friction forces, we consider water droplets in nonpatterned CNTs of varying wettability. A constant force is applied on all oxygen atoms, and the droplet is left to move until the interfacial friction force between water and CNT equals the driving force. At this stage, the composite force applied to the droplet is zero and an equilibrium terminal velocity is achieved.

We extract the friction coefficient for each combination of CNT length and radius by performing a set of six simulations, varying the applied force on the water molecules. This is repeated for four different values of surface wettability of the CNT (varying the interaction strength $\epsilon_{CO}$) and for three different CNT radii and three different CNT lengths (overall, a set of 144 simulations). From the constrained MD simulations, a scaling law is derived, relating the friction factor of water and CNTs to the interaction strength $\epsilon_{CO}$ and the radius $R$ of the CNT. This global scaling law is later exploited to obtain the instantaneous friction force in the unconstrained set of simulations, given the instantaneous CoM position.

The production runs of unconstrained MD simulations are conducted with equilibrated water droplets placed in CNTs with a gradient of stepwise wettability along their axis. The temperature of the water molecules is kept constant with a Nosè−Hoover thermostat,[66] adjusting only the thermal component of temperature, which was shown to be equivalent to a simulation in the NVE ensemble (see SI, Section 1.3). The droplets are driven into motion in the direction of the surface wettability gradient, corresponding to a gradient of surface energy, under the influence of interfacial forces.

The baseline simulation consists of a DW-CNT with chiralities of the inner and outer CNTs (20, 20) and (25, 25), respectively, denoting the DW-CNT chirality (20, 20) @(25, 25) and of length $L$ = 50 nm and a droplet length $L_d$ = 6 nm. We first study how the variation of the length of the water volume affects the kinetic characteristics of its motion, including its maximum velocity, $V_{CoM,max}$, in a patterned double-walled CNT, varying the length of the droplet but maintaining a constant wettability gradient. Next, we study the effect of the CNT radius, and hence also the water volume, maintaining the original length of both the tube and the droplet and varying their common radius. The parameters of the variably sized systems for all simulation cases, i.e., length $L$ and inner radius $R$ of the CNT, as well as the length of the droplet $L_d$ and number of water droplet molecules $N_{H_2O}$, are listed in Table S1 in SI. All utilized droplets are equilibrated in CNTs with the carbon−oxygen interaction strength equal to $\epsilon_{CO}$ = 0.0937 kcal/mol, which corresponds to a contact angle of a water droplet in a carbon nanotube equal to 95°.

Finally, from the production set of simulations of water droplets in patterned CNTs, we investigate how the dynamics of the moving droplet due to surface wettability pattern scale with its size. Throughout the entire motion, the acting force on the water droplet $F_{acc}$ is given as

$$F_{acc} = F_{dr} - F_{fr} = ma \tag{1}$$

where $m$ is the mass of the droplet and $a$ is its instantaneous acceleration.

It is known[67] that the Laplace force on the contact line of a droplet with a capillary conduit is related to wettability through the contact angle of the solid−liquid interface

$$F_{Laplace} = 2\pi R\gamma \cos\theta \tag{2}$$

where $\gamma$ is the surface tension of water.[68,69] The driving force of the water droplet originates from the gradient of wettability between the different annular zones along the length of the CNT and is given by

$$F_{dr} = F_{Laplace,adv} - F_{Laplace,rec} = 2\pi R\gamma(\cos\theta_{adv} - \cos\theta_{rec}) \tag{3}$$

where the subscripts adv and rec denote the advancing and the receding contact angles, respectively.

On the other hand, the friction force at the liquid/solid interface is given by

$$F_{fr} = \lambda A_{inter} V_{CoM} \tag{4}$$

where $\lambda$ is the interfacial friction coefficient, and $A_{inter}$ is the area of the solid−liquid contact, i.e., $A_{inter} \approx 2\pi RL_d$.

It is well known that the friction coefficient is a function of the CNT radius, whereas, for larger radii, this quantity converges to the friction coefficient on planar graphene.[24] Therefore, the friction force overall has a nonlinear dependency on the CNT radius and is proportional to the length of the CNT.

Moreover, the contact angle depends on the curvature of the interface in a nonlinear way[67,70] (see more in SI, Section 3). Conclusively, the driving Laplace force only depends on the radius, since for every length studied here, the aspect ratio of the droplet length and the width of each axial zone remains the same, i.e., the wettability gradient remains fixed.

In the manuscript, we investigate the scaling of the Laplace driving force of the droplets due to surface wettability pattern of the CNT and the scaling of the friction force with the variation of the length and radius of the water droplets. We extract the instantaneous net force accelerating the droplet $F_{acc,sim}$ directly from simulations as the sum of the pair forces between carbon and oxygen atoms for three lengths and three radii (in total six simulations, each of 2 ns). The force is responsible for the acceleration of the droplet and is denoted as $F_{acc,sim}$.

The instantaneous friction force $F_{fr}$ is calculated from the instantaneous droplet velocity and the friction coefficient that corresponds to the wettability zone the droplet experiences. We deduce a scaling law of the friction coefficient as a function of wettability and CNT radius with a set of constrained MD simulations of water flow in CNTs of varying surface areas and wettabilities. The instantaneous driving force $F_{dr}$ is finally calculated by adding the friction force $F_{fr}$ to the overall force $F_{acc,sim}$ for the instantaneous velocity and position of the droplet along the axis of the CNT ($F_{dr} \approx F_{acc,sim} + F_{fr}$).

## RESULTS AND DISCUSSION

We investigate the self-propulsion of water droplets through nanopores with a lengthwise surface wettability gradient; the baseline system is shown in Figure 1, and the simulation and postprocessing setup are presented in the Methods section.

We study how the transport characteristics of water droplets in nanopores with surface patterns vary with varying the sizes



https://doi.org/10.1021/acs.jpcb.1c07562
J. Phys. Chem. B XXXX, XXX, XXX−XXX

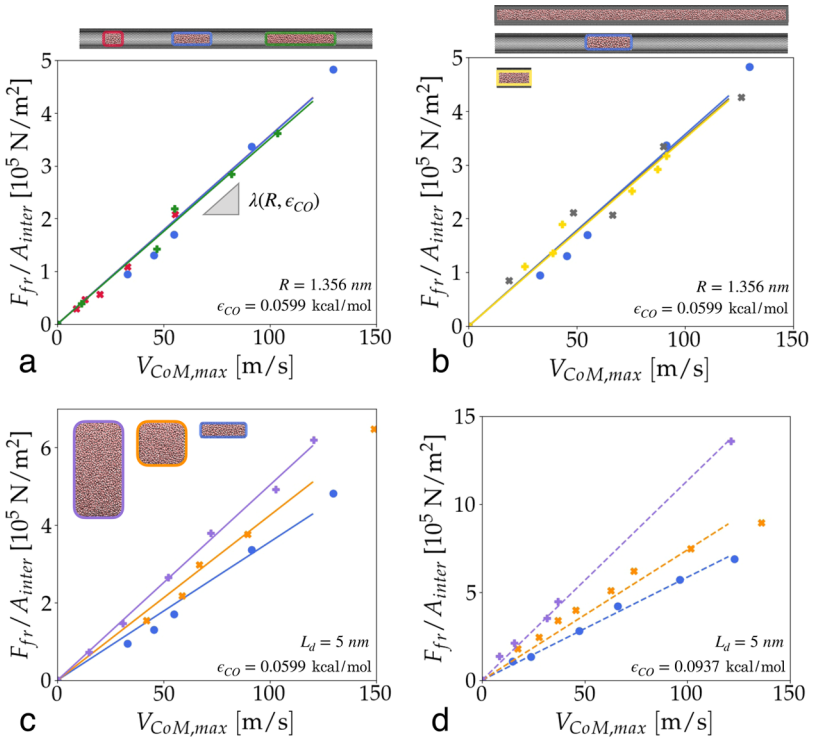


**Figure 2.** Friction coefficient of water in carbon nanotubes of different radii, droplet lengths, and wettabilities. (a, b) Effect of length: normalized friction force with the wetted area $F_{fr}/A$ *vs* terminal velocity $V_{CoM,max}$ of a droplet for a periodic CNT of chirality (20, 20)@(25, 25), $L$ = 50 nm, and surface wettability that corresponds to $\epsilon_{CO}$ = 0.0599 kcal/mol, (a) with $L$ = 50 nm and varying lengths of the water droplet: red corresponds to $L_d$ = 3 nm, blue to $L_d$ = 6 nm, and green to $L_d$ = 12 nm, (b) with varying lengths of CNT and water volume: blue corresponds to $L$ = 50 nm and $L_d$ = 6 nm, gray to $L = L_d$ = 50 nm, and yellow to $L = L_d$ = 6 nm. (c, d) Effect of radius: normalized friction force with the wetted area $F_{fr}/A$ *vs* terminal velocity $V_{CoM,max}$ of a droplet for a periodic CNT of length $L$ = 50 nm and surface wettability that corresponds to $\epsilon_{CO}$ = 0.0599 kcal/mol and $\epsilon_{CO}$ = 0.0937 kcal/mol for subfigures (c) and (d), respectively. In both panels (c) and (d), the colored curves correspond to different CNT inner radii $R$: blue curves correspond to $R$ = 1.356 nm, orange to $R$ = 3.391 nm, and purple to $R$ = 6.781 nm. The blue markers in all subfigures denote the reference CNT and droplet size combination.

(radius and length) and the structural characteristics of surface patterns (number of wettability zones and local wettability gradient) of the nanotubes and find that their actuated motion can be described by interfacial forces between the water droplet and the confining wall. As will be shown in the following sections, the introduction of scaling laws to describe the driving Laplace pressure and the friction forces of water in CNTs assists in expressing the transport of water droplets in patterned nanotubes through interfacial dynamics.

**Water Friction in Carbon Nanotubes.** Using molecular dynamics (MD) simulations, we estimate how water friction in CNTs changes with droplet length and radius in a CNT of uniform wettability, where a pre-specified force applied to the water molecules drives the fluid at a terminal equilibrium velocity (see the Methods section).

*Variation of Droplet Length and Radius.* With simulations for CNTs of different surface wettabilities, we study how the variation of droplet length and wall surface energy affect the friction coefficient. The employed CNT has an inner radius $R$ = 1.356 nm and a baseline length $L$ = 50 nm. For every surface wettability tested, the magnitude of the friction force normalized with the droplet/CNT contact area is proportional to the terminal velocity of the droplet $V_{CoM,max}$ (SI, Figure S4). The curves of the normalized friction force for varying droplet lengths ($L_d$ = 3, 6, 12 nm) collapse in one, as seen in Figure 2a. The slope of the curve designates the friction coefficient. In Figure 2a, for the value of interaction strength $\epsilon_{CO}$ = 0.0599 kcal/mol, this slope translates to a friction coefficient $\lambda$ = 3311 ± 24 (N s)/m$^3$. This outcome matches previous studies on the dependency of the friction coefficient on the droplet length.[33] We also find that for various droplet lengths and $R$ = 1.356 nm, there is an almost linear dependency of the calculated normalized friction $\lambda$ on surface wettability (SI, Figure S5).

Furthermore, we test the effect of the meniscus presence on the friction coefficient for three combinations of $L$ and $L_d$: (a) $L$ = 50 nm, $L_d$ = 6 nm; (b) $L$ = 6 nm, periodic and fully filled with water, $L_d$ = 6 nm; and (c) $L$ = 50 nm, periodic and fully filled with water, $L_d$ = 50 nm. In principle, these settings correspond to a CNT of infinity length, filled with water from end to end and to a CNT filled with a droplet of length $L_d$. We find that the friction coefficient $\lambda$ is modified less than 8% by the presence of a meniscus line, irrespectively of the surface wettability, as the curves of normalized friction force *vs* terminal velocity of the confined water approximately collapse into one, as in Figure 2b (for a more complete analysis, see SI, Section 2.2).

We further investigate how the variation of CNT radius affects the friction coefficient. For every surface wettability tested, the magnitude of the friction force is linearly proportional to the resulting terminal velocity of the droplet $V_{CoM,max}$. In contrast to the variation in droplet length, the curves of the normalized friction force *vs* droplet terminal velocities do not collapse onto each other (Figure 2c,2d), and the slope is different for varying surface wettabilities. Therefore, the friction coefficient $\lambda$ is a function of the interaction strength between carbon and oxygen atoms $\epsilon_{CO}$,


https://doi.org/10.1021/acs.jpcb.1c07562
J. Phys. Chem. B XXXX, XXX, XXX−XXX

i.e., the surface wettability, and the CNT radius $\lambda(R, \epsilon_{CO})$ (see SI, Section 2.3).

*Friction Coefficient Scaling Law.* Based on the above results, we deduce that the friction coefficient $\lambda$ has a nonlinear relation with the interaction strength $\epsilon_{CO}$ and the CNT radius (Figure 3). We construct a universal scaling law of the friction coefficient for water transport in CNTs of varying radii and wettabilities, with inspiration drawn from the studies of Thomas and McGaughey[20] and Suk and Aluru,[14] where the friction coefficient was considered as the quotient of the dynamic viscosity and the slip length $\mu(R)/L_s(R)$.

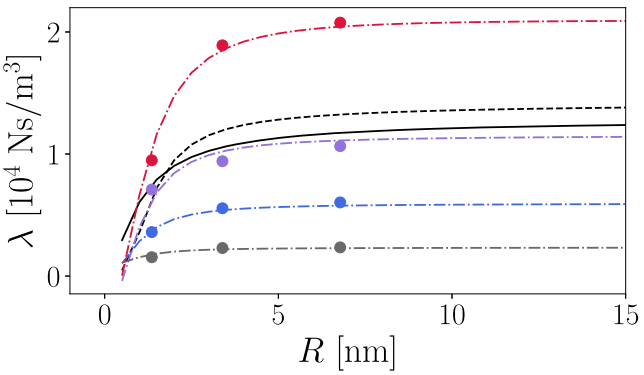


**Figure 3.** Friction coefficient $\lambda$ of water transported in CNTs of radius $R$ and surface wettability corresponding to $\epsilon_{CO}$. Dashed-dotted lines denote the scaling law of eq 5, optimized with the method of Martin et al.[71] The colored dot symbols correspond to friction coefficient values derived from MD simulations. Curve and symbol colors correspond to different values of $\epsilon_{CO}$: gray to $\epsilon_{CO}$ = 0.0299 kcal/mol, blue to $\epsilon_{CO}$ = 0.0599 kcal/mol, purple to $\epsilon_{CO}$ = 0.0937 kcal/mol, and red to $\epsilon_{CO}$ = 0.139 kcal/mol. The black dashed line corresponds to $\mu(R)/L_s(R)$ from Thomas and McGaughey,[20] and the black line corresponds to $\mu(R)/L_s(R)$ from Suk and Aluru.[14]

We conclude that the friction coefficient $\lambda$ of water in a CNT of radius $R$ and wettability that corresponds to $\epsilon_{CO}$ is described by

$$\lambda(R, \epsilon_{CO}) = (A\epsilon_{CO} + B)\epsilon_{CO} + \frac{C\epsilon_{CO}^2}{1 + R^d} \quad (5)$$

where the coefficients $A$, $B$, $C$, and $d$ were optimized with the help of the uncertainty quantification (UQ) framework developed within the CSE-Lab, `Korali`[71] (see SI, Section 2.3 for details). The optimization was performed with the CMA-ES algorithm, with resulting values from the computational model: $A = 68.95 \times 10^4 \frac{Ns}{m^3(kcal/mol)^2}$, $B = 5.585 \times 10^4 \frac{Ns}{m^3(kcal/mol)}$, $C = -165.5 \times 10^{-14} \frac{Ns}{m(kcal/mol)^2}$, $d = 2.0$. This scaling law, along with the values of friction coefficients obtained from the simulations, is plotted in Figure 3 and shows excellent agreement.

**Dynamics of Droplet Transport in Patterned CNTs.** The MD simulations of water droplets through patterned CNTs with the surface pattern, as described in Figure 1, predict that the droplets are self-propelled in ultrafast speeds through the CNT under the influence of the surface energy gradient, reaching maximum velocities on the order of 100 m/s and traveling the whole length of the tube in a time span of some ns, as shown in Figure 4.

The motion of the droplets under the imposed wettability gradient in the CNTs displays two distinct regimes.[30,33] In the first regime, the droplet moves in an accelerating manner, as the driving force $F_{dr}$ due to the Laplace pressure from the wettability gradient overpowers the hindering friction force $F_{fr}$ at the water and carbon interface. In the second regime, the velocity of the droplet reaches a terminal value, when the driving and the friction forces balance each other, whereas thereafter, the velocity further declines under the influence of the increasing friction force. We note that for the systems of

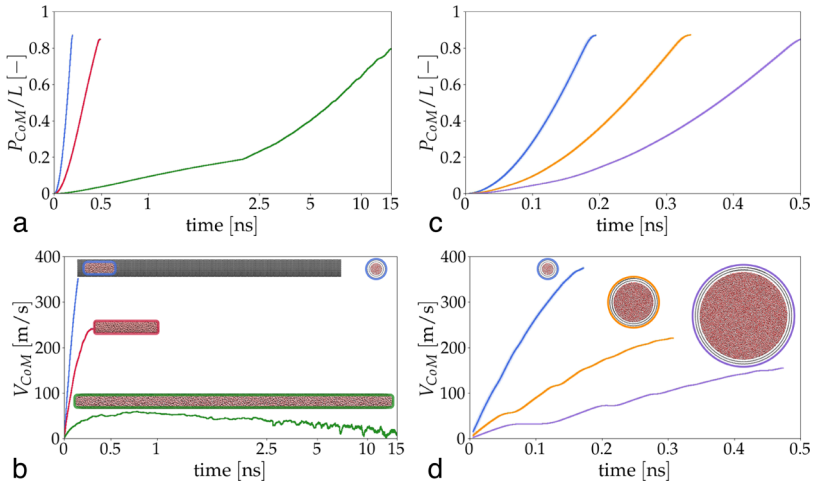


**Figure 4.** (a, c) Droplet center-of-mass position ($P_{CoM}$) normalized with the CNT length ($L$), and (b, d) respective velocity ($V_{CoM}$) *vs* time for water droplets of varying lengths (a, b) and varying radii (c, d). All cases are actuated with a CNT wettability gradient, as described in Figure 1. (a, b) The colored curves refer to different lengths of the droplets $L_d$ and the CNTs $L$ for $R$ = 1.356 nm: blue corresponds to $L$ = 50 nm, red to $L$ = 100 nm, and green to $L$ = 500 nm. The time axis is logarithmic. (c, d) The colored curves refer to different inner radii of the CNTs and consecutively of the droplet, for $L$ = 50 nm: blue corresponds to $R$ = 1.356 nm, orange to $R$ = 3.391 nm, and purple to $R$ = 6.781 nm. The blue curves refer to the baseline system for all subfigures. The graphs extend up to the point when the droplets reach the end of the nanopore. The curves are the averages of five simulations. The standard deviation is too small to be observed in the graph.



https://doi.org/10.1021/acs.jpcb.1c07562
J. Phys. Chem. B XXXX, XXX, XXX−XXX

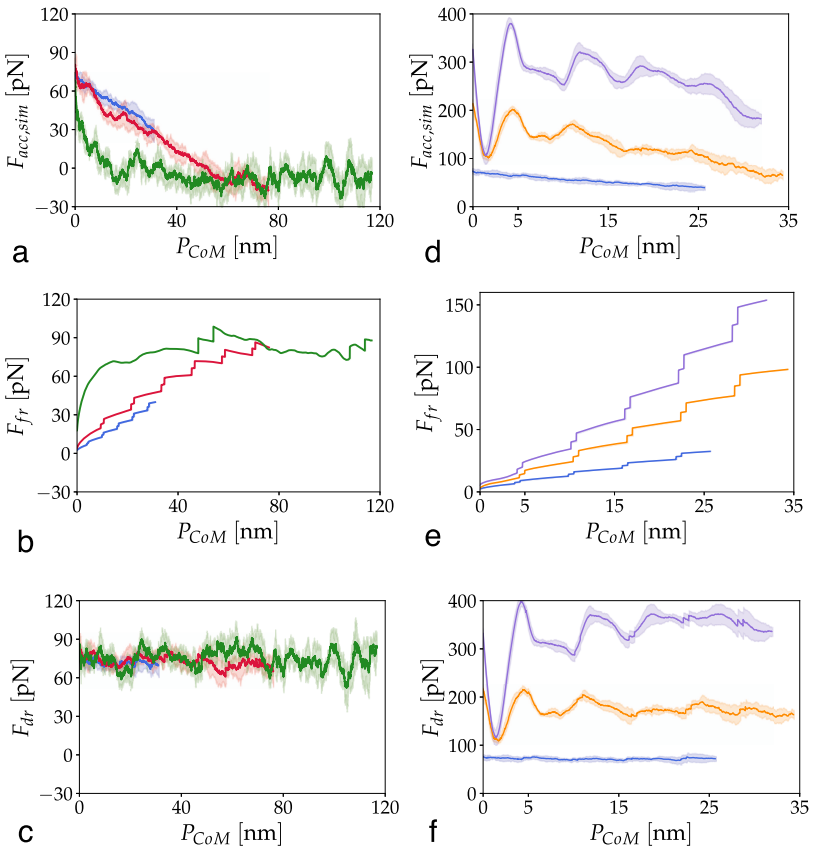


**Figure 5.** Instantaneous net accelerating force $F_{acc,sim}$ from simulations (a, d), friction force $F_{fr}$ (b, e), and resulting driving force $F_{dr} = F_{acc,sim} + F_{fr}$ (c, f) *vs* the CoM position $P_{CoM}$ of three droplets in patterned CNTs of various lengths (a−c) or radii (d−f) but with the same wettability gradient. (a−c) The colored curves refer to different lengths of the droplets and the CNT: blue corresponds to $L$ = 50 nm, red to $L$ = 100 nm, and green to $L$ = 500 nm. (d−f) The colored curves refer to different droplet/CNT radii: blue corresponds to $R$ = 1.356 nm, orange to $R$ = 3.391 nm, and purple to $R$ = 6.781 nm. Each solid line is the average of five MD simulations with the same conditions. The lighter-shaded region around each solid curve depicts the standard deviation of the sample. The blue curves are for the baseline system of CNT and droplet in all subfigures.

periodic patterned CNTs, the water droplet velocity will further decrease as the water droplet reaches the far end of the CNT under the influence of the hydrophobic zones of the periodic image.

We consider three water droplets of increasing $L$ and $L_d$ (but constant $L/L_d$ ratio), equilibrated in neutrally wettable nanotubes of the same inner radius $R$ (see SI, Table S1). The droplets are released in CNTs of length $L$, whose surface wettability is patterned in an axial gradient, as in Figure 1. The wettability gradient remains constant unless otherwise stated. We place the water droplets at the same initial relative position to the CNT end to ensure the same initial acceleration.

The temporal evolution of the center-of-mass position $P_{CoM}$ and velocity $V_{CoM}$ of the droplets is derived from the simulation trajectories (Figure 4a,4b). The water droplets are driven into motion in the direction of the wettability gradient (lower-to-higher surface wettability). From the three cases considered, the droplets with lengths $L_d$ = 12 and 60 nm reach a constant velocity in the final stage of the shown trajectory.

We further consider CNTs of varying radii. Three droplets of the same length $L_d$ = 6 nm are equilibrated in neutrally wettable CNTs of increasing radii $R$ = 1.356, 3.391, and 6.781 nm, as listed in Table S1 in SI. The droplets are then released in CNTs of the aforementioned radii and length $L$ = 50 nm, with the same linear surface wettability gradient of Figure 1. It is apparent that the curvature affects both the driving and friction forces. The droplets are induced into motion in the direction of the wettability gradient, with acceleration decreasing for larger radii, due to their larger mass and contact area with the CNT wall, which translates to larger friction (Figure 4c,4d).

We find that the equilibration of the water droplet before release does not significantly affect its kinematics through the patterned CNT (see SI, Section 2.4). The trajectories of two droplets, one equilibrated in a neutrally wettable CNT (static contact angle $\theta_S$ = 90°) and the second equilibrated in a hydrophobic CNT (front contact angle $\theta_{S,fr}$ = 125°), vary by less than 6% in terms of their peak CoM velocity. On the other hand, we find that varying the local wettability gradient $\delta\epsilon_{CO}/\delta z$, by varying the number of steps, affects the axial droplet trajectory less than 8%, whereas an increase of the end-to-end wettability difference $\Delta\epsilon_{CO}$ of the patterned CNT by 66% results in 33% higher $V_{CoM,max}$. An increase of the wettability gradient increases both the driving and friction forces along the CNT length; therefore, the relation between the wettability gradient and the maximum velocity is not linearly analogous (see SI, Sections 2.5 and 2.6).

We now explore the dynamics of water droplets released into patterned CNTs with varying lengths and radii. The instantaneous net droplet force $F_{acc}$ is derived from the simulations and induces a motion of declining acceleration, regardless of the droplet length (Figure 5a,d). We note that for larger radii, oscillations of the droplet's $F_{acc}$ correspond to oscillations of the droplet's CoM. As the droplet traverses


https://doi.org/10.1021/acs.jpcb.1c07562
J. Phys. Chem. B XXXX, XXX, XXX−XXX

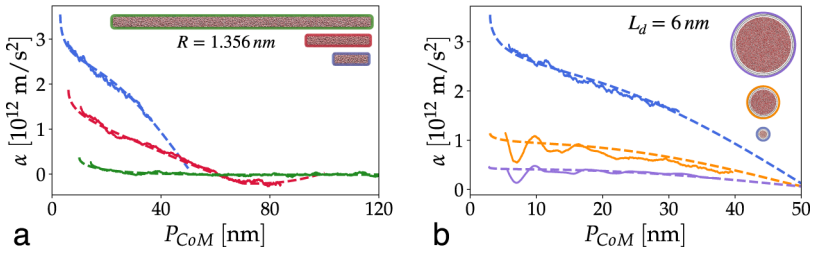


**Figure 6.** Acceleration of water droplets in CNTs patterned with the same wettability gradient $\Delta\epsilon_{CO}$ = 0.16 − 0.04 kcal/mol; MD simulation results are shown as solid curves (each is the average of five MD simulations), while the values from the analytical model eqs 8 and 4 are shown as dashed lines. In panel a the colored curves refer to different lengths of the droplets $L_d$ for a CNT inner radius $R$ = 1.356 nm: blue corresponds to $L_d$ = 6 nm, red to $L_d$ = 12 nm, and green to $L_d$ = 60 nm. In panel b, the colored curves refer to different CNT inner radii $R$ for $L_d$ = 6 nm and $L$ = 50 nm: blue corresponds to $R$ = 1.356 nm, orange to $R$ = 3.391 nm, and purple to $R$ = 6.781 nm. The blue curve is the same in both subfigures.

through a zone of new wettability, the interfacial region of water is transformed, to adapt to the new wettability, inducing waveforms on the free surface of the droplet at the liquid−vacuum interface. The droplet's CoM reacts to the interfacial shape reformation with a time lag. These oscillations of the droplet's CoM due to the interfacial shape transformation are inherent in all systems, but more evident for larger radii, as the water volume close to the interface with the CNT corresponds to a smaller percentage of the entire water volume of the droplet (see SI, Section 4).

The instantaneous friction force between the carbon surface and the water molecules hinders the droplet motion and is derived using the scaling law obtained between friction coefficient $\lambda$, interaction strength $\epsilon_{CO}$, and the CNT radius $R$ eq 5, given the droplets' CoM positions and velocities (Figure 5b,5e). The friction force increases for larger velocities. The sum of the net force and the friction force provides the driving force, i.e., the Laplacian force, due to the wettability gradient along the CNT axis, $F_{dr} = F_{acc} + F_{fr}$ (Figure 5c,5f), which depends on the droplet's position. The average of the driving force $F_{dr}$ coincides for all tested droplet lengths and same radius. On the other hand, the variation of radius modifies the resulting $F_{dr}$. This is attributed to the contact angle difference when the CNT radius changes.

**Analytical Model of Interfacial Forces.** So far, we have quantified the effect of surface wettability gradient along the length of nanotubes on the kinematics of water droplets induced into motion under the influence of interfacial forces between carbon and water. The droplet kinematic behavior varies with the size of the droplet and the CNT, as well as with the inherent wettability gradient. Here, we construct an analytical model of the interfacial forces acting on the droplet to accurately predict the scaling of the kinematic behavior of a droplet of length $L_d$ released in a CNT of length $L$ and inner radius $R$. The contact area between carbon and water is $A_{inter} = 2\pi RL_d$. The CNT has a positive linear wettability gradient, i.e., the CNT wall surface changes from hydrophobic to hydrophilic. As before, the wettability is defined through the interaction strength between carbon and oxygen $\epsilon_{CO}$ and end-values of $\epsilon_0$ and $\epsilon_1$, where $\epsilon_0 = \epsilon(z_0)$ and $\epsilon_1 = \epsilon(z_1)$

$$\epsilon_{CO}(z) = \epsilon_0 + \frac{\epsilon_1 - \epsilon_0}{L}(z - z_0) \tag{6}$$

The droplet motion is affected by two counteracting forces. The friction force $F_{fr}$ between water molecules and the carbon wall opposes the droplet motion and depends on the surface wettability; namely, it increases as the droplet reaches more hydrophilic zones. The friction force depends on the friction coefficient between liquid and solid, the contact area between the droplet and the CNT wall, and the CoM velocity of the droplet

$$F_{fr}(P_{CoM}, V_{CoM}) = \lambda[\epsilon_{CO}(P_{CoM}), R]A_{inter}V_{CoM} \tag{7}$$

As shown earlier, the friction coefficient $\lambda$ depends on the surface wettability and the effective CNT radius. In all cases, the effective CNT radius is computed as the radius of the inner CNT, subtracting half the interaction cutoff distance $\sigma_{CO}$ between liquid and the solid wall. Through the friction study, we derived a scaling law between the friction coefficient and the surface wettability and CNT curvature, i.e., the CNT radius eq 5. Here, it is assumed that the instantaneous friction coefficient of the water droplet is the average of the maximum and minimum $\lambda$ between the zones that the water droplet is in contact. Furthermore, the instantaneous friction coefficient between water and each wettability zone is assumed to be equal to the respective equilibrium value of a droplet in a CNT of the same uniform wettability.

On the other hand, the driving force $F_{dr}$ stems from the wettability gradient along the CNT length and it is defined as

$$\begin{aligned} F_{dr}(P_{CoM}) &= 2\pi R\gamma\Delta\cos(\theta_D) \\ &= 2\pi R\gamma(\cos\theta_{D,adv} - \cos\theta_{D,rec}) \end{aligned} \tag{8}$$

where $\gamma$ = 71.73 mN/m, the surface tension of water, and $\theta_{D,adv}$ and $\theta_{D,rec}$ are the advancing and receding dynamic contact angles of the water droplet at the interface of the CNT wall, respectively.

We find that the scaling of the driving force cannot be captured with the measured difference of the corresponding static contact angles $\theta_S$ at the advancing and receding sides of the droplet throughout its motion. We therefore consider the dynamic contact angle $\theta_D$, which corrects the static contact angle for a moving droplet, taking into consideration the contribution of the capillary number $Ca = \mu V_{CoM}/\gamma$, where $\mu$ is the dynamic viscosity of water in a CNT of radius $R$, taken from Suk and Aluru.[14] The static contact angle depends on the wettability of the tube at the advancing and receding sides of the droplet $\theta_S(\epsilon_{CO})$. In the literature, there are numerous models describing the dynamic contact angle,[72−75] and many of these have been successfully used for droplets on planar surfaces with various combinations of fluid and solid elements. However, all previous models of the dynamic contact angle were only applicable to droplet transport under small capillary numbers. Here, we introduce a simple linear scaling between the dynamic contact angle, the static contact angle, and the capillary number


https://doi.org/10.1021/acs.jpcb.1c07562
J. Phys. Chem. B XXXX, XXX, XXX−XXX

$$\theta_D(\theta_S, V_{CoM}) = a_1\theta_S + a_2\frac{\mu V_{CoM}}{\gamma} + a_3 \quad (9)$$

which is fitted to the existing simulation results for the driving force of the droplet

$$F_{dr}(P_{CoM}, V_{CoM}) = 2\pi R\gamma[\cos(\theta_D(\theta_S(\epsilon_{CO}(P_{CoM} + 0.5L_d)), V_{CoM})) - \cos(\theta_D(\theta_S(\epsilon_{CO}(P_{CoM} - 0.5L_d)), V_{CoM}))] \quad (10)$$

with $L_d$ = 6 nm, $L$ = 50 nm, and $R$ = 1.356 nm, deducing $a_1$ = 0.6834, $a_2$ = 11.41°, and $a_3$ = 34.72° for the coefficients of eq 9 with optimization in Korali.[71] The derivation of the expressions of the dynamic contact angle, the friction, and the driving forces can be found in the SI, Section 3. Finally, we calculate the resulting instantaneous accelerating force $F_{acc}(P_{CoM}, V_{CoM}) = F_{dr}(P_{CoM}, V_{CoM}) - F_{fr}(P_{CoM}, V_{CoM})$. As indicated by the relations for $F_{dr}$ and $F_{fr}$ (eqs 7 and 10), the interfacial forces acting on a droplet transported in a stepwise patterned nanotube are expressed in terms of the instantaneous position and velocity of the CoM of the moving droplet.

We can, therefore, use the analytical forcing model to integrate the equations of motion and describe the dynamics of a droplet moving in a CNT featuring a lengthwise surface wettability gradient. We solve Newton's equation of motion for the droplet using the present expression for $F_{acc}$ through a leap-frog time integration. Figure 6 reveals that this analytical model, which utilizes the newly proposed scaling law for the friction coefficient (eq 5) and the dynamic contact angle (eq 9) of water droplets in CNTs, can accurately predict the dynamic transport of droplets along wettability-patterned CNTs.

We perform a scaling analysis of the dynamics of the droplet's motion under the influence of the CNT surface pattern using the proposed analytical model in SI, Section 3.1, where we show that the variation in the "normalized" force $F_{fr,/,dr}/2\pi R$, where $F_{dr} = F_{fr}$ with the radius of the droplet, is reduced for smaller applied wettability gradient. We note that the analytical model captures the mean dynamic behavior of the droplet but not the oscillatory behavior of the droplet, as it is a simple one-dimensional model, not taking into consideration the local phenomena at the interface. Nevertheless, the model may be of universal value in predicting the response of water droplets of various sizes in nanomembranes that feature different surface wettability patterns by omitting computationally expensive simulations.

## CONCLUSIONS

We have presented ultrafast transport of water droplets inside carbon nanotubes with varying wall wettabilities, without any externally imposed pressure gradients, with droplet velocities of $O(100)$ m/s and accelerations of $O(10^{10})$ g. Our studies entail large-scale molecular dynamics simulations revealing how the interplay between friction and the wettability gradient forces governs the droplet transport along the CNT. We find that the magnitude of the driving force due to surface wettability gradient is not velocity-dependent and varies nonlinearly with the droplet radius. We present a scaling law for the dynamic contact angle of water droplets in CNTs with varying surface wettabilities, which is then employed to describe the capillary force actuating the droplet to move rapidly along a CNT with a stepwise surface wettability gradient.

We investigate in detail the scaling of the friction of water in CNTs of varying sizes and conclude that the friction coefficient is not dependent on the droplet length nor is it altered by the presence of a meniscus. We derive a universal scaling law to relate the friction coefficient to the surface wettability and the curvature of the confining nanotube. The present results confirm previous experimental and computational studies of water enhancement through nanopores by modeling directly the friction mechanism between the wall and water in contrast to slip length. We show that the increase of the pore radius and the wettability of the solid wall lead to an increase in the friction between the solid and the liquid. This is equivalent to the decrease of the water flow slip length and consecutively the flow ability, i.e., water flow enhancement. The proposed scaling law of friction can describe the dual relationship of the water flow enhancement with the dimension and surface wettability of the confining nanopore.

We employ the friction coefficient law to describe the instantaneous friction force of a moving droplet along a CNT with a patterned surface. We then construct an analytical model that captures the dynamics of the motion of droplets of varying sizes in carbon nanopores of varying surface wettabilities. The results of this study will assist the future design of efficient selective membranes, as they reveal simple and universally applied scaling laws to model the friction and capillary forces for the transport of water droplets. Finally, the present study suggests the potential of patterned CNTs as ultraefficient water nanopumps that can be realized for applications in water filtration and nanomedicine.

## ASSOCIATED CONTENT

### Supporting Information

The Supporting Information is available free of charge at https://pubs.acs.org/doi/10.1021/acs.jpcb.1c07562.

Droplet preparation; cutoff distance of short-range interactions; effect of thermostatting; effect of phonon excitation of the carbon atoms; complementary graphs for the friction of droplets in CNTs; uncertainty of friction coefficient; effect of water droplet equilibration; effect of the number of wettability zones; effect of wettability gradient; analytical forcing model; and uncertainty quantification for static and dynamic contact angle scaling relations (PDF)

## AUTHOR INFORMATION


### Corresponding Author

**Petros Koumoutsakos** − *John A. Paulson School of Engineering and Applied Sciences, Harvard University, Cambridge, Massachusetts 02138, United States; Computational Science and Engineering Laboratory, ETH Zürich, Zürich CH-8092, Switzerland;* orcid.org/0000-0001-8337-2122; Email: petros@seas.harvard.edu.

### Authors

**Ermioni Papadopoulou** − *Computational Science and Engineering Laboratory, ETH Zürich, Zürich CH-8092, Switzerland*

**Constantine M. Megaridis** − *Department of Mechanical and Industrial Engineering, University of Illinois at Chicago,*




https://doi.org/10.1021/acs.jpcb.1c07562
J. Phys. Chem. B XXXX, XXX, XXX−XXX

*Chicago, Illinois 60607, United States;* orcid.org/0000-0002-6339-6933

**Jens H. Walther** − *Computational Science and Engineering Laboratory, ETH Zürich, Zürich CH-8092, Switzerland; Department of Mechanical Engineering, Technical University of Denmark, 2800 Kongens Lyngby, Denmark*

Complete contact information is available at: https://pubs.acs.org/10.1021/acs.jpcb.1c07562

### Author Contributions

E.P., J.H.W., C.M.M., and P.K. designed the study and the MD campaign. E.P. performed the MD simulations and the analysis of the MD results. C.M.M., J.H.W., and P.K. coordinated the project and participated in the analysis of the results. All authors contributed to the writing and editing of the manuscript.

### Notes

The authors declare no competing financial interest.

## ■ ACKNOWLEDGMENTS

The authors acknowledge the Swiss National Supercomputing Centre (CSCS) for computing time through project s930.

## ■ REFERENCES

(1) De Jong, W. H.; Borm, P. J. A. Drug Delivery and Nanoparticles: Applications and Hazards. *Int. J. Nanomed.* **2008**, *3*, 133−149.
(2) Wang, Z. M.; Waag, A.; Salamo, G.; Kishimoto, N.; Bellucci, S.; Park, Y. J. *Nanoscale Sensors*; Springer, 2013.
(3) De Volder, M. F. L.; Tawfick, S. H.; Baughman, R. H.; Hart, A. J. Carbon Nanotubes: Present and Future Commercial Applications. *Science* **2013**, *339*, 535−540.
(4) Shannon, M. A.; Bohn, P. W.; Elimelech, M.; Georgiadis, J. G.; Marin, B. J.; Mayes, A. M. Science and Technology for Water Purification in the Coming Decades. *Nature* **2008**, *452*, 301−310.
(5) Corry, B. Designing Carbon Nanotube Membranes for Efficient Water Desalination. *J. Phys. Chem. B.* **2008**, *112*, 1427−1434.
(6) Tîlmaciu, C. M.; Morris, M. C. Carbon Nanotube Biosensors. *Front. Chem.* **2015**, *3*, 59.
(7) Walther, J. H.; Werder, T.; Jaffe, R. L.; Koumoutsakos, P. Hydrodynamic Properties of Carbon Nanotubes. *Phys. Rev. E* **2004**, *69*, No. 062201.
(8) Sparreboom, W.; van den Berg, A.; Eijkel, J. C. T. Principles and Applications of Nanofluidic Transport. *Nat. Nanotechnol.* **2009**, *4*, 713−720.
(9) Hummer, G.; Rasaiah, J. C.; Noworyta, J. P. Water Conduction through the Hydrophobic Channel of a Carbon Nanotube. *Nature* **2001**, *414*, 188−190.
(10) Holt, J. K.; Park, H. G.; Wang, Y.; Stadermann, M.; Artyukhin, A. B.; Grigoropoulos, C. P.; Noy, A.; Bakajin, O. Fast Mass transport through Sub−2-Nanometer Carbon Nanotubes. *Science* **2006**, *312*, 1034−1037.
(11) Majumder, M.; Chopra, N.; Andrews, R.; Hinds, B. J. Enhanced Flow in Carbon Nanotubes. *Nature* **2005**, *438*, 44.
(12) An, A. K.; Lee, E. J.; Guo, J.; Jeong, S.; Lee, J. G.; Ghaffour, N. Enhanced Vapor Transport in Membrane Distillation via Functionalized Carbon Nanotubes anchored into Electrospun Nanofibres. *Sci. Rep.* **2017**, *7*, No. 41562.
(13) Li, Y.; Li, Z.; Aydin, F.; Quan, J.; Chen, X.; Yao, Y. C.; Zhan, C.; Chen, Y.; Pham, T. A.; Noy, A. Water-Ion Permselectivity of Narrow-diameter Carbon Nanotubes. *Sci. Adv.* **2020**, *6*, No. eaba9966.
(14) Suk, M. E.; Aluru, N. R. Modeling Water Flow Through Carbon Nanotube Membranes with Entrance/Exit Effects. *Nanoscale Microscale Thermophys. Eng.* **2017**, *21*, 247−262.
(15) Thomas, M.; Corry, B. A computational assessment of the permeability and salt rejection of carbon nanotube membranes and their application to water desalination. *Philos. Trans. R. Soc., A* **2016**, *374*, No. 20150020.
(16) Zeng, H.; Wu, K.; Cui, X.; Chen, Z. Wettability Effect on Nanoconfined Water Flow: Insights and Perspectives. *Nano Today* **2017**, *16*, 7−8.
(17) Thomas, J. A.; McGaughey, A. J. H. Density, Distribution and Orientation of Water Molecules inside and outside Carbon Nanotubes. *J. Chem. Phys.* **2008**, *128*, No. 084715.
(18) Hassan, J.; Diamantopoulos, G.; Homouz, D.; Papavasiliou, G. Water inside Carbon Nanotubes: Structure and Dynamics. *Nanotechnol. Rev.* **2016**, *5*, 341−354.
(19) Varghese, S.; Kannam, S. K.; Hansen, J. S.; Sathian, S. P. Effect of Hydrogen Bonds on the Dielectric Properties of Interfacial Water. *Langmuir* **2019**, *35*, 8159−8166.
(20) Thomas, J. A.; McGaughey, A. J. H. Reassessing Fast Water Transport through Carbon Nanotubes. *Nano Lett.* **2008**, *8*, 2788−2793.
(21) Falk, K.; Sedlmeier, F.; Joly, L.; Netz, R. R.; Bocquet, L. Molecular Origin of Fast Water Transport in Carbon Nanotube Membranes: Superlubricity versus Curvature Dependent Friction. *Nano Lett.* **2010**, *10*, 4067−4073.
(22) Secchi, E.; Marbach, S.; Niguès, A.; Stein, D.; Siria, A.; Bocquet, L. Massive Radius-dependent Flow Slippage in Single Carbon Nanotubes. *Nature* **2016**, *537*, 210−213.
(23) Tocci, G.; Joly, L.; Michaelides, A. Friction of Water on Graphene and Hexagonal Boron Nitride from Ab Initio Methods: Very Different Slippage Despite Very Similar Interface Structures. *Nano Lett.* **2014**, *14*, 6872−6877.
(24) Falk, K.; Sedlmeier, F.; Joly, L.; Netz, R. R.; Bocquet, L. Ultralow Liquid/Solid Friction in Carbon Nanotubes: Comprehensive Theory for Alcohols, Alkanes, OMCTS, and Water. *Langmuir* **2012**, *28*, 14261−14272.
(25) Björneholm, O.; Hansen, M. H.; Hodgson, A.; Liu, L. M.; Limmer, D. T.; Michaelides, A.; Pedevilla, P.; Rossmeisl, J.; Shen, H.; Tocci, G.; et al. Water at Interfaces. *Chem. Rev.* **2016**, *116*, 7698−7726.
(26) Zhang, L.; Wu, J.; Hedhili, M. N.; Yang, X.; Wang, P. Inkjet Printing for Direct Micropatterning of a Superhydrophobic Surface: toward Biomimetic Fog Harvesting Surfaces. *J. Mater. Chem. A* **2015**, *3*, 2844−2852.
(27) Bhushan, B.; Jung, Y. C. Natural and Biomimetic Artificial Surfaces for Superhydrophobicity, Self-Cleaning, Low Adhesion, and Drag Reduction. *Prog. Mater. Sci.* **2011**, *56*, 1−108.
(28) Corletto, A.; Shapter, J. G. Nanoscale Patterning of Carbon Nanotubes: Techniques, Applications, and Future. *Adv. Sci.* **2021**, *8*, No. 2001778.
(29) Breynaert, E.; Houlleberghs, M.; Radhakrishnan, S.; Grübel, G.; Taulelle, F.; Martens, J. A. Water as a Tuneable Solvent: a Perspective. *Chem. Soc. Rev.* **2020**, *49*, 2557.
(30) Shiomi, J.; Maruyama, S. Water Transport inside a Single-walled Carbon Nanotube Driven by a Temperature Gradient. *Nanotechnology* **2009**, *20*, No. 055708.
(31) Zambrano, H. A.; Walther, J. H.; Koumoutsakos, P.; Sbalzarini, I. F. Thermophoretic Motion of Water Nanodroplets Confined inside Carbon Nanotubes. *Nano Lett.* **2009**, *9*, 66−71.
(32) Rajegowda, R.; Kannam, S. K.; Hartkamp, R.; Sathian, S. P. Thermophoretic Transport of Ionic Liquid Droplets in Carbon Nanotubes. *Nanotechnology* **2017**, *28*, No. 155401.
(33) Oyarzua, E.; Walther, J. H.; Zambrano, H. A. Water Thermophoresis in Carbon Nanotubes: the Interplay between Thermophoretic and Friction Forces. *Phys. Chem. Chem. Phys.* **2018**, *20*, 3672.
(34) Zhang, C.; Lu, P.; Chen, Y. Molecular Dynamics Simulation of Electroosmotic Flow in Rough Nanochannels. *Int. Commun. Heat Mass Transfer* **2014**, *59*, 101−105.
(35) Cui, W.; Ma, H.; Tian, B.; Ji, Y.; Su, F. Electrowetting on a Multi-walled Carbon Nanotube Membrane with Different Droplet Sizes in an Electric Field. *J. Mater. Sci.* **2016**, *51*, 4031−4036.

(36) Zhou, K. G.; Vasu, K. S.; Cherian, C. T.; Neek-Amal, M.; Zhang, J. C.; Ghorbanfekr-Kalashami, H.; Huang, K.; Marshall, O. P.; Kravets, V. G.; Abraham, J.; et al. Electrically Controlled Water Permeation through Graphene Oxide Membranes. *Nature* **2018**, *559*, 236−240.
(37) Roh, J. S.; Lee, H.; Lee, T. H.; Yoon, H. W.; Choi, T. H.; Do, S.; Yoo, S. Y.; Freeman, B. D.; Song, T.; Paik, U.; et al. Unprecedentedly Low $CO_2$ Transport through Vertically Aligned, Conical Silicon Nanotube Membranes. *Nano Lett.* **2020**, *20*, 4754−4760.
(38) Werder, T.; Walther, J. H.; Jaffe, R. L.; Halicioglu, T.; Koumoutsakos, P. On the Water-Carbon Interaction for Use in Molecular Dynamics Simulations of Graphite and Carbon Nanotubes. *J. Phys. Chem. B.* **2003**, *107*, 1345−1352.
(39) Zhang, M.; Zhang, T.; Cui, T. Wettability Conversion from Superoleophobic to Superhydrophilic on Titania/Single-walled Carbon Nanotube Composite Coatings. *Langmuir* **2011**, *27*, 9295−9301.
(40) Li, H.; Lai, Y.; Huang, J.; Tang, Y.; Yang, L.; Chen, Z.; Zhang, K.; Wang, X.; Tan, L. P. Multifunctional Wettability Patterns prepared by Laser Processing on Superhydrophobic $TiO_2$ Nanostructured Surfaces. *J. Mater. Chem. B* **2015**, *3*, 342−347.
(41) Nagayama, G.; Cheng, P. Effects of Interface Wettability on Microscale Flow by Molecular Dynamics Simulation. *Int. J. Heat Mass Transfer* **2004**, *47*, 501−513.
(42) Yang, S. C. Effects of Surface Roughness and Interface Wettability on Nanoscale Flow in a Nanochannel. *Microfluid. Nanofluid.* **2006**, *2*, 501−511.
(43) Chatterjee, R.; Bhattacharjee, S.; Mitra, S. K. Particle Transport in Patterned Cylindrical Microchannels. *Microfluid. Nanofluid.* **2012**, *12*, 41−51.
(44) Nicholls, W. D.; Borg, M. K.; Lockerby, D. A.; Reese, J. M. Water Transport through Carbon Nanotubes with Defects. *Mol. Simul.* **2012**, *38*, 781−785.
(45) Moskowitz, I.; Snyder, M. A.; Mittal, J. Water Transport through Functionalized Nanotubes with Tunable Hydrophobicity. *J. Comput. Phys.* **2014**, *141*, No. 18C532.
(46) Melillo, M.; Zhu, F.; Snyder, M. A.; Mittal, J. Water Transport through Nanotubes with Varying Interaction Strength between Tube Wall and Water. *J. Phys. Chem. Lett.* **2011**, *2*, 2978−2983.
(47) Kou, J.; Mei, M.; Lu, H.; Wu, F.; Fan, J. Unidirectional Motion of a Water Nanodroplet Subjected to a Surface Energy Gradient. *Phys. Rev. E.* **2012**, *85*, No. 056301.
(48) Zhang, K.; Wang, F.; Lu, Y. Molecular Dynamics Simulation of Continuous Nanoflow Transport through the Uneven Wettability Channel. *AIP Adv.* **2018**, *8*, No. 015111.
(49) Ghosh, A.; Ganguly, R.; Schutzius, T. M.; Megaridis, C. M. Wettability Patterning for High-rate, Pumpless Fluid Transport on Open, Non-planar Microfluidic Platforms. *Lab Chip* **2014**, *14*, 1538−1550.
(50) Li, Q.; Wu, D.; Guo, Z. Drop/bubble Transportation and Controllable Manipulation on Patterned Slippery Lubricant infused Surfaces with Tunable Wettability. *Soft Matter* **2019**, *15*, 6803.
(51) Papadopoulou, E.; Megaridis, C. M.; Walther, J. H.; Koumoutsakos, P. Ultrafast Propulsion of Water Nanodroplets on Patterned Graphene. *ACS Nano* **2019**, *13*, 5465−5472.
(52) Arai, N.; Koishi, T.; Ebisuzaki, T. Nanotube Active Water Pump Driven by Alternating Hydrophobicity. *ACS Nano* **2021**, *15*, 2481−2489.
(53) Werder, T.; Walther, J. H.; Jaffe, R. L.; Halicioglu, T.; Koumoutsakos, P. On the Water-Carbon Interaction for Use in Molecular Dynamics Simulations of Graphite and Carbon Nanotubes. *J. Phys. Chem. B* **2003**, *107*, 1345−1352.
(54) Angelikopoulos, P.; Papadimitriou, C.; Koumoutsakos, P. Data Driven, Predictive Molecular Dynamics for Nanoscale Flow Simulations under Uncertainty. *J. Phys. Chem. B* **2013**, *117*, 14808−14816.
(55) Horn, H. W.; Swope, W. C.; Pitera, J. W.; Madura, J. D.; Dick, T. J.; Hura, G. L.; Head-Gordon, T. Development of an Improved Four-site Water Model for Biomolecular Simulations: TIP4P-Ew. *J. Comput. Phys.* **2004**, *120*, 9665−9678.
(56) Deserno, M.; Holm, C. How to mesh up Ewald Sums I. A Theoretical and Numerical Comparison of Various Particle Mesh Routines. *J. Comput. Phys.* **1998**, *109*, 7678−7693.
(57) Kräutler, V.; van Gusteren, W. F.; Hünenberger, P. H. A Fast SHAKE Algorithm to Solve Distance Constraints for Small Molecules in Molecular Dynamics Simulations. *J. Comput. Chem.* **2001**, *22*, 501−508.
(58) Mayo, S. L.; Olafson, B. D.; Goddard, W. A. DREIDING: A Generic Force Field for Molecular Simulations. *J. Phys. Chem. A* **1990**, *94*, 8897−8909.
(59) Jorgensen, W. L.; Chandrasekhar, J.; Madura, J. D.; Impey, R. W.; Klein, M. L. Comparison of Simple Potential Functions for Simulating Liquid Water. *J. Chem. Phys.* **1983**, *79*, 926−935.
(60) Ma, M.; Tocci, G.; Michaelides, A.; Aeppli, G. Fast Diffusion of Water Nanodroplets on Graphene. *Nat. Mat.* **2016**, *15*, 66−72.
(61) Cruz-Chú, E. R.; Papadopoulou, E.; Walther, J. H.; Popadic, A.; Li, G.; Praprotnik, M.; Koumoutsakos, P. On Phonons and Water Flow Enhancement in Carbon Nanotubes. *Nat. Nanotechnol.* **2017**, *12*, 1106−1108.
(62) Plimpton, S. Fast Parallel Algorithms for Short-range Molecular Dynamics. *J. Comput. Phys.* **1995**, *117*, 1−19.
(63) Humphrey, W.; Dalke, A.; Schulten, K. VMD − Visual Molecular Dynamics. *J. Mol. Graphics.* **1996**, *14*, 33−38.
(64) WCCNT. https://github.com/cselab/wccnt (accessed Oct 29th 2016).
(65) Michaud-Agrawal, N.; Denning, E. J.; Woolf, T. B.; Beckstein, O. MDAnalysis: A Toolkit for the Analysis of Molecular Dynamics Simulations. *J. Comput. Chem.* **2011**, *32*, 2319−2327.
(66) Frenkel, D.; Smit, B. *Understanding Molecular Simulation*; Academic Press: San Diego, CA, 2002.
(67) Imadate, K.; Hirahara, K. Experimental Determination of the Diameter-dependent Wettability of Carbon Nanotubes as Studied using Atomic Force Microscopy. *Phys. Chem. Chem. Phys.* **2018**, *20*, 26979.
(68) Vega, C.; De Miguel, E. Surface Tension of the Most Popular Models of Water by Using the Test-area Simulation Method. *J. Comput. Phys.* **2007**, *126*, No. 154707.
(69) Alejandre, J.; Chapela, G. A. The Surface Tension of TIP4P/2005 Water Model using the Ewald Sums for the Dispersion Interactions. *J. Chem. Phys.* **2010**, *132*, No. 014701.
(70) Werder, T.; Walther, J. H.; Jaffe, R. L.; Halicioglu, T.; Noca, F.; Koumoutsakos, P. Molecular Dynamics Simulations of Contact Angles of Water Droplets in Carbon Nanotubes. *Nano Lett.* **2001**, *1*, 697−702.
(71) Martin, S. M.; Wälchli, D.; Arampatzis, G.; Economides, A. E.; Karnakov, P.; Koumoutsakos, P. Korali: a High-Performance Computing Framework for Stochastic Optimization and Bayesian Uncertainty Quantification. 2020; arXiv:2005.13457.
(72) Kistler, S. F. In *Wettability*; Berg, J. C., Ed.; Taylor & Francis Group: New York, 1993; p 311.
(73) Shikhmurzaev, Y. D. Mathematical Modeling of Wetting Hydrodynamics. *Fluid Dyn. Res.* **1994**, *13*, 45−64.
(74) Cox, R. G. The Dynamics of the Spreading of Liquids on a Solid Surface. Part 1. Viscous Flow. *J. Fluid Mech.* **1986**, *168*, No. 169194.
(75) Tanner, L. H. The Spreading of Silicone Oil Drops on Horizontal Surfaces. *J. Phys. D: Appl. Phys.* **1979**, *12*, 1473.


https://doi.org/10.1021/acs.jpcb.1c07562
J. Phys. Chem. B XXXX, XXX, XXX−XXX